IOP Publishing New J. Phys. 26 (2024) 113022 https://doi.org/10.1088/1367-2630/ad95b3

New Journal of Physics
The open access journal at the forefront of physics

Deutsche Physikalische Gesellschaft DPG
IOP Institute of Physics

Published in partnership with: Deutsche Physikalische Gesellschaft and the Institute of Physics

OPEN ACCESS

RECEIVED
21 August 2024

REVISED
13 November 2024

ACCEPTED FOR PUBLICATION
21 November 2024

PUBLISHED
2 December 2024

PAPER

Generation of non-Gaussian states of light using deterministic photon subtraction

Abdolreza Pasharavesh[1,2,*] **and Michal Bajcsy**[1,2]

[1] Institute for Quantum Computing, University of Waterloo, Waterloo, ON, Canada
[2] Department of Electrical and Computer Engineering, University of Waterloo, Waterloo, ON, Canada
[*] Author to whom any correspondence should be addressed.

E-mail: apashara@uwaterloo.ca and mbajcsy@uwaterloo.ca

Keywords: deterministic photon subtraction, single-photon Raman interaction, quantum state engineering, input–output formalism, Schrodinger's kitten states

Abstract

We explore a recently demonstrated deterministic photon subtraction scheme, based on single-photon Raman interaction with a Λ-type three-level atom, as a tool for manipulating quantum state of few-photon light pulses. We establish a comprehensive theoretical framework using input–output formalism and quantum regression theorem, enabling calculation of the first order autocorrelation matrices of the output light and identification of the temporal modes present in the generated light via their eigendecomposition. By modeling the entire system as a quantum network consisting multiple virtual cavities and a lambda-type emitter cascaded in two parallel guided modes of opposite propagation directions, we extract the quantum state occupying the modes of interest. For both squeezed vacuum and coherent light input pulses, the Wigner function of the output light after photon subtraction clearly reveals its non-Gaussian character. Furthermore, we propose a measurement-based scheme on the subtracted photon which can lead to conditional generation of quantum states resembling Schrodinger's kitten state directly from coherent input light with fidelities above 99%. This result is particularly nothworthy, as coherent pulses, unlike the squeezed vacuum inputs commonly used in previous studies, are readily available in most experimental setups.

1. Introduction

Discrete variable (DV) and continuous variable (CV) regimes represent distinct approaches in quantum optics. These two regimes are primarily characterized by the Hilbert spaces employed for the representation of quantum states of light. Within the DV approach, quantum states are typically illustrated in a finite-dimensional space, commonly associated with the polarization of single or multiple photons. Conversely, in the CV approach, individual spatiotemporal modes of light are treated as single harmonic oscillators. Their representation involves field quadrature components, such as position and momentum, within an infinite-dimensional Hilbert space [1]. Both of these approaches have evolved over time and demonstrated their inherent potential in various applications of quantum technologies including quantum communication [2], computing [3], and metrology [4]. In the context of CV quantum optics, quantum states are classified into two categories, called Gaussian and non-Gaussian, based on the shape of the probability distribution they exhibit in the optical phase space. The first group either occurs in nature, such as vacuum and thermal states, or can be experimentally generated on-demand, like coherent and squeezed states. On the other hand, the generation of non-Gaussian states of light with high fidelities remains experimentally challenging [5]. At the same time, a variety of applications in CV quantum optics explicitly require non-Gaussian states and non-Gaussian operators. For example, a no-go theorem demonstrates that achieving fault-tolerant quantum computing is not possible solely with Gaussian states and operations [6]. In another example, it has been shown that leveraging Schrödinger's cat state as a resource enables the realization of quantum error correction [7]. Similarly, non-Gaussian operators can enable CV entanglement

distillation [8], which is impossible in Gaussian regime based on another no-go theorem [9]. Additionally, non-Gaussian states find applications in long-distance communication using quantum repeaters and teleportation via entangled cat states [10], as well as in interfacing discrete-continuous regimes [11].

Harnessing the existing possibilities of quantum information in the above-mentioned applications requires the capability to produce light in different non-Gaussian quantum states. The quantum states in CV regime are superpositions or mixtures of Fock states with different numbers of photons. Consequently, the addition and subtraction of photons to or from an initial Gaussian state can be a potential method for creating non-Gaussian states of light. Traditionally, this has been done through application of creation and annihilation operators [12]. However, creation and annihilation operators do not exactly add or subtract single photons from arbitrary states and cannot be deterministically implemented. This arises from the fact that the annihilation and creation operators do not preserve the trace of the density matrix and, as a result, cannot be implemented in a system that evolves under a deterministic Hamiltonian [13]. Dakna *et al* [14] demonstrated that, starting from the vacuum state, any single-mode state of light can be generated through the alternate application of photon creation and displacement operators. Similarly, Fiurasek *et al* [15] showed that the same level of control can be achieved using the photon annihilation operator in combination with displacement and squeezing operations. It should be noted that the non-deterministic nature of these methods can lead to very low success probabilities in the generation process of the desired quantum state. Regarding non-deterministic photon subtraction, the first successful experimental implementation was reported in 2004 by Wenger *et al* [16]. They achieved the subtraction of single photons from traveling waves using a heralded scheme consisting of a low-reflectivity beamsplitter. Using pulses of squeezed light as the input, the non-Gaussian statistics of the output light was clearly demonstrated in their work by reconstruction of the Wigner function from the experimental data. Later in 2007, Ourjoumtsev *et al* carried out the same experiment with an optimized homodyne detection and were able to observe Wigner functions with negative values, resembling the Schrodinger's kitten state [17].

In 2016, Rosenblum *et al* proposed and experimentally demonstrated a photon subtraction scheme, capable of deterministically extracting one photon from any arbitrary input quantum state [18]. The device operated based on single photon Raman interaction (SPRINT) with a Λ-type atom. Although the capability of an ideal deterministic single photon subtractor in generating non-Gaussian states of light was previously proposed by Honer *et al* [19], there is currently no known experimental scheme that can precisely implement this operator. Similar to other methods which subtract the first arriving photon, the SPRINT mechanism produces a multimode output even when supplied with a single-mode input pulse. While this downside limits the deterministic generation of pure states, SPRINT still offers potential for non-Gaussian manipulation of quantum states. In this paper, we conduct a comprehensive analysis of the SPRINT-based photon subtraction process to assess its potential in the generation of non-Gaussian states of light. The considered scheme involves a chiral waveguide directly coupled to a Λ-type atom [20, 21]. Our analysis employs the input–output formalism in two distinct stages. First, we calculate the first-order coherence matrices to extract the mode shapes present in the output pulses. Next, we use the results of the first step to model the device as a cascaded atom-cavity quantum network and determine its effective Hamiltonian and Lindblad operators. Finally, we employ the quantum trajectory method to simulate the system and derive the quantum states generated by the photon-subtracting device.

2. Theoretical formulation

A SPRINT-based photon subtractor relies on a three-level Λ-type atom, where distinct ground-to-excited state transitions are selectively coupled to two different light modes. These modes may correspond to either distinct modes within a bimodal cavity [18] or counterpropagating bath of modes within a chiral waveguide [20]. Figure 1 schematically depicts the latter design employing a chiral waveguide which is directly interacting with the atom. Modes propagating in different directions are represented by distinct colors, with their correspondence to atomic transitions highlighted in the same color. Consider the atom initially prepared in ground state $|1\rangle$, with the input light directed towards the right propagating mode (depicted in green). During the Raman interaction, the atom first absorbs a single photon from the input light, becoming excited. Subsequently, the destructive interference between the atom's emission into the same mode as the input light causes it to decay to the other ground state [22]. This transition results in the emission of a single photon into the left propagating mode (depicted in red), effectively subtracting one photon from the input pulse in a deterministic manner. Following this interaction, the atom remains in state $|2\rangle$, where it no longer interacts with the input light.

Here we use input–output formalism to analytically study the interaction of the atom with the bath of waveguide modes during the photon subtraction process. This gives a set of differential equations governing evolution of the atomic operators $\sigma_{ij} = |i\rangle\langle j|$ in the Heisenberg picture as a function of the input operators

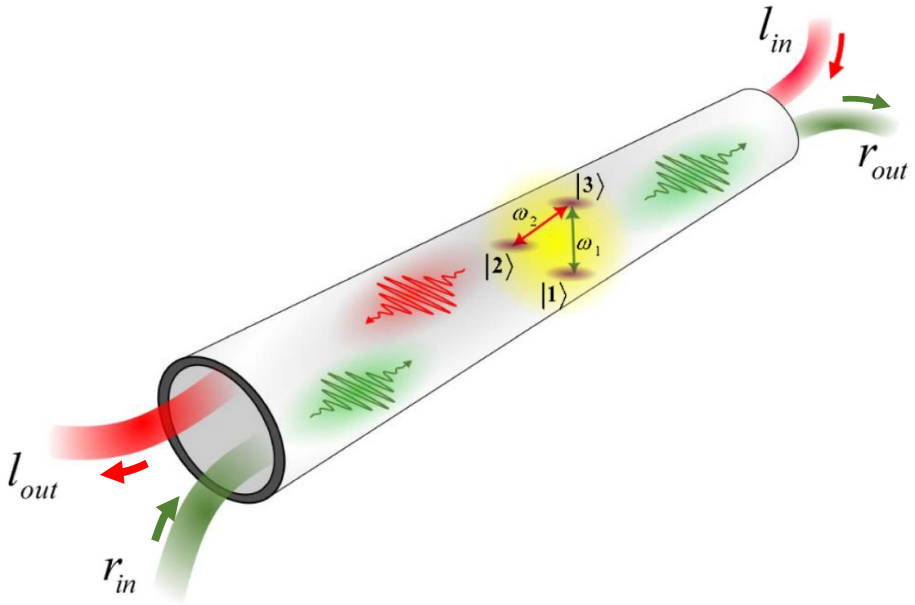

Figure 1. Schematic view of a Λ-type atom coupled to a chiral waveguide. The input pulse is sent to the right-propagating (green) mode, the subtracted photon is reflected to the left-propagating (red) mode, while the remaining pulse leaves the waveguide from the same mode's output.

$r_{\text{in}}(t)$ and $l_{\text{in}}(t)$:

$$\begin{aligned}
\partial_t\sigma_{11} &= \sqrt{\gamma_g}\left(\sigma_{31}r_{\text{in}} + r_{\text{in}}^{\dagger}\sigma_{13}\right) + \gamma_g\sigma_{33}\\
\partial_t\sigma_{22} &= \sqrt{\gamma_g}\left(\sigma_{32}l_{\text{in}} + l_{\text{in}}^{\dagger}\sigma_{23}\right) + \gamma_g\sigma_{33}\\
\partial_t\sigma_{33} &= -\sqrt{\gamma_g}\left(\sigma_{31}r_{\text{in}} + r_{\text{in}}^{\dagger}\sigma_{13}\right) - \sqrt{\gamma_g}\left(\sigma_{32}l_{\text{in}} + l_{\text{in}}^{\dagger}\sigma_{23}\right) - 2\gamma_g\sigma_{33}\\
\partial_t\sigma_{13} &= -i\omega_1\sigma_{13} + \sqrt{\gamma_g}\left(\sigma_{33} - \sigma_{11}\right)r_{\text{in}} - \sqrt{\gamma_g}\sigma_{12}l_{\text{in}} - \gamma_g\sigma_{13}\\
\partial_t\sigma_{23} &= -i\omega_2\sigma_{23} + \sqrt{\gamma_g}\left(\sigma_{33} - \sigma_{22}\right)l_{\text{in}} - \sqrt{\gamma_g}\sigma_{21}r_{\text{in}} - \gamma_g\sigma_{23}\\
\partial_t\sigma_{12} &= -i\left(\omega_1 - \omega_2\right)\sigma_{12} + \sqrt{\gamma_g}\sigma_{32}r_{\text{in}} + \sqrt{\gamma_g}l_{\text{in}}^{\dagger}\sigma_{13}.
\end{aligned} \tag{1}$$

In the above equation ω_i is the transition frequency from the excited state to the ground state $|i\rangle$ and γ_g denotes the emission rate of the atom to the guided modes of the waveguide. In addition, the corresponding inputs and outputs of the system are connected by the following relations:

$$r_{\text{out}} = r_{\text{in}} + \sqrt{\gamma_g}\sigma_{13} \qquad l_{\text{out}} = l_{\text{in}} + \sqrt{\gamma_g}\sigma_{23}. \tag{2}$$

The details on derivation of equations (1) and (2) are provided in appendix A.

We assume that the input light is sent to the r_{in} mode and l_{in} is initially in vacuum state. Also, the emitter is in its ground state $|1\rangle$ at $t = t_0$ before the light interacts with the emitter. Therefore, According to the photon subtraction scenario described above, l_{out} contains the subtracted single photon and r_{out} represents the remaining light after subtraction of a single photon. In the pulsed operation regime, where both the input and output of the device consist of pulses of light with finite durations, the initial step in the quantum state analysis of the output light is to conduct a modal decomposition to distinguish the potentially involved temporal modes at each output. Consider a set of temporal modes identified by their complex mode amplitude functions $h_j(t)$, which represent the temporal shape of each wave-packet, where j indexes the mode number. A photon wave-packet annihilation operator A_j can be defined for each mode as the following superposition [23, 24]:

$$A_j = \int h_j(t)\, a_t \mathrm{d}t \tag{3}$$

where $a_t = (1/\sqrt{2\pi})\int a_\omega \exp(-\mathrm{i}\omega t)\,\mathrm{d}\omega$ is the annihilation operator that annihilates a photon at time t. It can be shown that if h_j forms a set of orthonormal functions, satisfying $\int h_i^*(t)\, h_j(t)\,\mathrm{d}t = \delta_{ij}$, then the

wave-packet annihilation operators obey the bosonic commutation relation $\left[A_i, A_j^\dagger\right] = \delta_{ij}$ just as a_ω or a_t do. This allows us to express the quantum state of the light in its most general form as follows:

$$|\psi\rangle = \bigotimes_{i=1}^{n} |\psi_i\rangle \tag{4}$$

where $|\psi_i\rangle = \sum_j (c_{ij}/\sqrt{j!})(A_i^\dagger)^j |0\rangle$ denotes the quantum state of light in the ith temporal mode, and n represents the number of modes in which all, or, using an approximation, the majority of photons exist. The elements c_{ij} are components of a matrix containing the superposition coefficients. Additionally, using the above representation, the mean number of photons existing in the ith mode is given by:

$$\bar{n}_i = \langle\psi_i \left| A_i^\dagger A_i \right| \psi_i\rangle = \sum_j j \left|c_{ij}\right|^2. \tag{5}$$

Using equation (3), the first-order autocorrelation function $G^{(1)}(t_2, t_1) = \left\langle a_{t_2}^\dagger a_{t_1} \right\rangle$ for a light field in the quantum state $|\psi\rangle$, as given in equation (4), can be written as follows:

$$G^{(1)}(t_2, t_1) = \left(\bigotimes_{i=1}^{n} \langle\psi_i|\right) a_{t_2}^\dagger a_{t_1} \left(\bigotimes_{i=1}^{n} |\psi_i\rangle\right) = \sum_{i=1}^{n} \bar{n}_i h_i^*(t_1) h_i(t_2). \tag{6}$$

The above equation suggests that an effective way to identify an appropriate set of orthonormal modes for a light field is through the eigendecomposition of its first-order autocorrelation matrix [25]. In this process, the resulting eigenvectors form the orthonormal mode function set, and their corresponding eigenvalues indicate the mean number of photons in each mode. The unnormalized first autocorrelation functions for l_{out} and r_{out} modes, by definition, are [26]:

$$\begin{aligned} G_l^{(1)}(t_2, t_1) &= \left\langle l_{\text{out}}^\dagger(t_2)\, l_{\text{out}}(t_1) \right\rangle \\ G_r^{(1)}(t_2, t_1) &= \left\langle r_{\text{out}}^\dagger(t_2)\, r_{\text{out}}(t_1) \right\rangle \end{aligned} \tag{7}$$

which after substituting equation (2), results in:

$$\begin{aligned} G_l^{(1)}(t_2, t_1) &= \gamma_g \langle \sigma_{32}(t_2)\, \sigma_{23}(t_1) \rangle \\ G_r^{(1)}(t_2, t_1) &= \gamma_g \langle \sigma_{31}(t_2)\, \sigma_{13}(t_1) \rangle + \langle {r_{\text{in}}}^\dagger(t_2)\, r_{\text{in}}(t_1) \rangle + \sqrt{\gamma_g} \langle {r_{\text{in}}}^\dagger(t_2)\, \sigma_{13}(t_1) \rangle + \sqrt{\gamma_g} \langle \sigma_{31}(t_2)\, r_{\text{in}}(t_1) \rangle \end{aligned} . \tag{8}$$

To find $G_{r,l}^{(1)}$, we use quantum regression theorem. Based on this theorem, if there exists a complete set of system operators A_μ, $\mu = 1, 2, \ldots$ such that:

$$\frac{\mathrm{d}}{\mathrm{d}t} \langle A_\mu(t) \rangle = \sum_\lambda M_{\mu\lambda} \langle A_\lambda(t) \rangle \tag{9}$$

for a two-point correlation, like the ones appeared in equation (8), one can write [27]:

$$\frac{\mathrm{d}}{\mathrm{d}t_2} \langle A_\mu(t_2)\, O(t_1) \rangle = \sum_\lambda M_{\mu\lambda} \langle A_\lambda(t_2)\, O(t_1) \rangle. \tag{10}$$

To assess the performance of the single photon subtractor, we examine three distinct input pulses: Fock state pulse, squeezed vacuum pulse, and coherent pulse. Initially, consider an n-photon Fock state pulse with carrier frequency ω_1 and a wavepacket amplitude of $\alpha(t)$ sent to the input mode r_{in}. By sandwitching the optical Bloch equation (1) between the input n-photon Fock state $|n\rangle$, the following sets of recurrence differential equations governing the time evolution of the expectation values $\langle \sigma_{ab} \rangle = {}_n\langle \sigma_{ab} \rangle_n = \langle n | \sigma_{ab} | n \rangle$ are derived:

$$\begin{aligned} \partial_t \langle \sigma_{11} \rangle &= \sqrt{\gamma_g} \left({}_n\langle \sigma_{31} \rangle_{n-1} \alpha(t) + \alpha^*(t) {}_{n-1}\langle \sigma_{13} \rangle_n \right) \sqrt{n} + \gamma_g \langle \sigma_{33} \rangle \\ \partial_t \langle \sigma_{33} \rangle &= -\sqrt{\gamma_g} \left({}_n\langle \sigma_{31} \rangle_{n-1} \alpha(t) + \alpha^*(t) {}_{n-1}\langle \sigma_{13} \rangle_n \right) \sqrt{n} - 2\gamma_g \langle \sigma_{33} \rangle \\ \partial_t \langle \sigma_{13} \rangle &= \sqrt{\gamma_g} \left({}_n\langle \sigma_{33} \rangle_{n-1} - {}_n\langle \sigma_{11} \rangle_{n-1} \right) \sqrt{n} \alpha(t) - \gamma_g \langle \sigma_{13} \rangle \\ \partial_t \langle \sigma_{31} \rangle &= \sqrt{\gamma_g} \left({}_{n-1}\langle \sigma_{33} \rangle_n - {}_{n-1}\langle \sigma_{11} \rangle_n \right) \sqrt{n} \alpha^*(t) - \gamma_g \langle \sigma_{31} \rangle \\ \partial_t \langle \sigma_{32} \rangle &= -\sqrt{\gamma_g} {}_{n-1}\langle \sigma_{12} \rangle_n \sqrt{n} \alpha^*(t) - \gamma_g \langle \sigma_{32} \rangle \\ \partial_t \langle \sigma_{12} \rangle &= \sqrt{\gamma_g} {}_n\langle \sigma_{32} \rangle_{n-1} \sqrt{n} \alpha(t) \end{aligned} . \tag{11}$$

In deriving the above equation, we used the relation $r_{\text{in}}(t)|n\rangle = \sqrt{n}\alpha(t)|n-1\rangle$. To calculate the expectation value $\langle\sigma_{ij}\rangle$, one needs to first derive differential equations for all terms of the form ${}_i\langle\sigma_{ab}\rangle_j = \langle i|\sigma_{ab}|j\rangle$, where both i and j vary between 0 and n. This results in a set of $6(n+1)^2$ coupled equations which can be numerically integrated with the initial condition of ${}_i\langle\sigma_{11}\rangle_i = 1$. Also, according to equations (9) and (10), similar sets of equations are derived for the first correlation terms appeared in the right-hand side of equation (8) i.e. $\langle\sigma_{32}(t_2)\sigma_{23}(t_1)\rangle$ and $\langle\sigma_{31}(t_2)\sigma_{13}(t_1)\rangle$:

$$\begin{aligned}
\partial_{t_2}\langle\sigma_{11}(t_2)\sigma_{13}(t_1)\rangle &= \sqrt{\gamma_g}\left({}_n\langle\sigma_{31}(t_2)\sigma_{13}(t_1)\rangle_{n-1}\alpha(t_2) + \alpha^*(t_2)\,{}_{n-1}\langle\sigma_{13}(t_2)\sigma_{13}(t_1)\rangle_n\right)\\
&\quad\times\sqrt{n} + \gamma_g\langle\sigma_{33}(t_2)\sigma_{13}(t_1)\rangle\\
\partial_{t_2}\langle\sigma_{33}(t_2)\sigma_{13}(t_1)\rangle &= -\sqrt{\gamma_g}\left({}_n\langle\sigma_{31}(t_2)\sigma_{13}(t_1)\rangle_{n-1}\alpha(t_2) + \alpha^*(t_2)_{n-1}\langle\sigma_{13}(t_2)\sigma_{13}(t_1)\rangle_n\right)\\
&\quad\times\sqrt{n} - 2\gamma_g\langle\sigma_{33}(t_2)\sigma_{13}(t_1)\rangle\\
\partial_{t_2}\langle\sigma_{13}(t_2)\sigma_{13}(t_1)\rangle &= \sqrt{\gamma_g}\left({}_n\langle\sigma_{33}(t_2)\sigma_{13}(t_1)\rangle_{n-1}\alpha(t_2) - \alpha^*(t_2)\,{}_n\langle\sigma_{11}(t_2)\sigma_{13}(t_1)\rangle_{n-1}\right)\\
&\quad\times\sqrt{n} - \gamma_g\langle\sigma_{13}(t_2)\sigma_{13}(t_1)\rangle\\
\partial_{t_2}\langle\sigma_{31}(t_2)\sigma_{13}(t_1)\rangle &= \sqrt{\gamma_g}\left({}_{n-1}\langle\sigma_{33}(t_2)\sigma_{13}(t_1)\rangle_n - {}_{n-1}\langle\sigma_{11}(t_2)\sigma_{13}(t_1)\rangle_n\right)\sqrt{n}\alpha^*(t_2) - \gamma_g\langle\sigma_{31}(t_2)\sigma_{13}(t_1)\rangle\\
\partial_{t_2}\langle\sigma_{32}(t_2)\sigma_{23}(t_1)\rangle &= -\sqrt{\gamma_g}{}_{n-1}\langle\sigma_{12}(t_2)\sigma_{23}(t_1)\rangle_n\sqrt{n}\alpha^*(t_2) - \gamma_g\langle\sigma_{32}(t_2)\sigma_{23}(t_1)\rangle\\
\partial_{t_2}\langle\sigma_{12}(t_2)\sigma_{23}(t_1)\rangle &= \sqrt{\gamma_g}{}_n\langle\sigma_{32}(t_2)\sigma_{23}(t_1)\rangle_{n-1}\sqrt{n}\alpha(t_2)
\end{aligned} \tag{12}$$

which are derived based on the commutation relation $\left[\sigma_{ij}(t_1), r_{\text{in}}(t_2)\right] = 0$ for $t_2 > t_1$, as a result of causality [28]. Equation (12) needs to be integrated from $t_2 = t_1$ according to the following initial conditions:

$$\begin{aligned}
{}_i\langle\sigma_{32}(t_2)\sigma_{23}(t_1)\rangle_j\Big|_{t_2=t_1} &= {}_i\langle\sigma_{31}(t_2)\sigma_{13}(t_1)\rangle_j\Big|_{t_2=t_1} = {}_i\langle\sigma_{33}(t_1)\rangle_j\\
{}_i\langle\sigma_{12}(t_2)\sigma_{23}(t_1)\rangle_j\Big|_{t_2=t_1} &= {}_i\langle\sigma_{11}(t_2)\sigma_{13}(t_1)\rangle_j\Big|_{t_2=t_1} = {}_i\langle\sigma_{13}(t_1)\rangle_j
\end{aligned}. \tag{13}$$

For the other three correlation terms appeared in equation (8), one can write:

$$\begin{aligned}
\langle r_{\text{in}}{}^\dagger(t_2)\,r_{\text{in}}(t_1)\rangle &= n\alpha^*(t_2)\alpha(t_1)\\
\langle r_{\text{in}}{}^\dagger(t_2)\sigma_{13}(t_1)\rangle &= \sqrt{n}\alpha^*(t_2)\,{}_{n-1}\langle\sigma_{13}(t_1)\rangle_n\\
\langle\sigma_{31}(t_2)\,r_{\text{in}}(t_1)\rangle &= {}_n\langle\sigma_{31}(t_2)\rangle_{n-1}\sqrt{n}\alpha(t_1).
\end{aligned} \tag{14}$$

When the input is a squeezed vacuum or coherent state, a similar analysis can be used to calculate the first autocorrelation matrices, with the detailed steps provided in Appendices B and C, respectively. After determining the modes included in the output light through eigen decomposition of the first-order coherence matrices, we follow the method proposed in [25]. to calculate the quantum state of the light in each mode. The method enables the modeling of each propagating wavepacket in the waveguide through a single virtual one-sided cavity with a time-dependent decay rate, coupled with the three-level emitter in a cascaded manner. The input cavity (with annihilation operator a_α) initially contains the quantum state of the input pulse sent to the photon subtractor, while the output cavities (with annihilation operators a_u^i and a_w^i) capture the quantum state contained at each output mode as the interaction occurs. Figure 2 shows a schematic view of the obtained quantum network, where only one cavity is depicted at each output port for simplicity. This network can be evolved over time by solving its governing master equation:

$$\frac{\mathrm{d}\rho}{\mathrm{d}t} = -i[H,\rho] + \sum_{i=0}\left(L_i\rho L_i^\dagger - \frac{1}{2}\left\{L_i^\dagger L_i,\rho\right\}\right) \tag{15}$$

with the following Hamiltonian and Lindblad operators in the rotating frame:

$$\begin{aligned}
H(t) &= \frac{i}{2}\left[\sqrt{\gamma_g}g_\alpha(t)\,a_\alpha^\dagger\sigma_{13} + \sqrt{\gamma_g}g_\nu^*(t)\,\sigma_{31}a_\nu + g_\alpha(t)\,g_\nu^*(t)\,a_\alpha^\dagger a_\nu + \sqrt{\gamma_g}g_w^*(t)\,\sigma_{32}a_w - \text{H.c.}\right]\\
L_0(t) &= \sqrt{\gamma_g}\sigma_{13} + g_\alpha^*(t)\,a_\alpha + g_\nu^*(t)\,a_\nu \qquad L_1(t) = \sqrt{\gamma_g}\sigma_{23} + g_w^*(t)\,a_w
\end{aligned} \tag{16}$$

L_0 and L_1 in the above equation are responsible for collapses when a photon, not in the main mode, is detected at the right and left propagating outputs, respectively. The time-dependent coupling of the cavities to their input continuum field is related to their corresponding wavepacket function according to the below relations:

$$g_\alpha(t) = \frac{\alpha^*(t)}{\sqrt{1-\int_0^t \mathrm{d}t'|\alpha(t')|^2}} \qquad g_x(t) = -\frac{x^*(t)}{\sqrt{\int_0^t \mathrm{d}t'|x(t')|^2}} \qquad x = \nu, w. \tag{17}$$

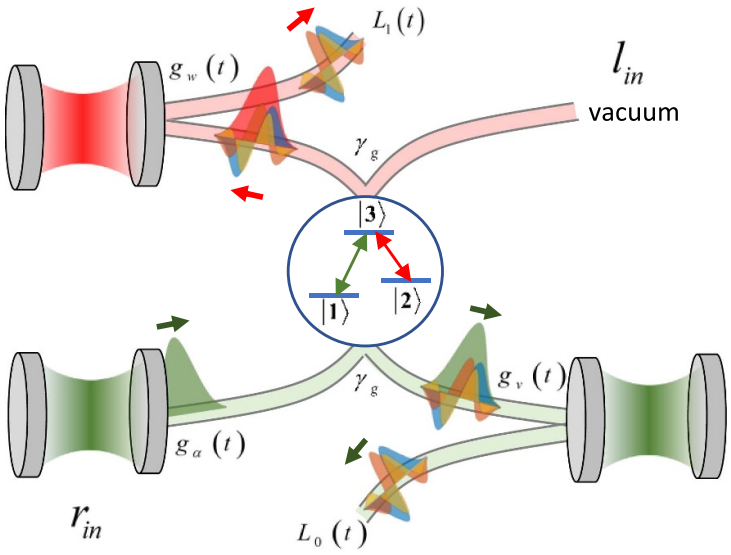

Figure 2. Quantum network comprising one input and two output cavities interacting with the emitter in a cascade manner. The couplings of the output cavities are adjusted so that they absorb the main wavepacket at each output pulse.

Here, $\alpha(t)$, as before, represents the wavepacket amplitude of the input pulse, while $v(t)$ and $w(t)$ denote the first mode shapes of the pulses leaving the system at the right and left propagating outputs, respectively. The above model can be extended for a higher number of cavities to capture additional modes at the outputs, following a similar framework based on the SLH method [29].

3. Results and discussion

In our simulations, we make the assumption that the input pulse has a Gaussian temporal shape. For the case of an input Fock or squeezed state, the temporal profile is modeled by the normalized form of a Gaussian function i.e. $\alpha(t) = \sqrt{2}\Big/\sqrt[4]{\pi\tau^2} \times \exp\left(-2t^2/\tau^2\right)$, while for the coherent pulse containing an average number of $\bar{n}$ photons, where $\alpha(t)$ essentially represents the phasor of the light pulse, we multiply it by $\sqrt{\bar{n}}$. As the first step, we employ the method described in the previous section to determine the first-order coherence matrices of the light at outputs r_{out} and l_{out}. Through an eigen-decomposition, we identify the modeshapes contained in each output. Results are illustrated in figures 3–6 for the three different types of input pulses. The legends of the plots indicate the number of photons in each eigenmode which are their corresponding eigenvalues. For enhanced visual representation of the photon distribution among modes, and to better illustrate the relative contribution of different modes to the final modal structure, the mode shapes are weighted by the square root of the contained photons. It should be noted that, because the input light applied to the system is a single-wavepacket pulse with a real-valued amplitude function, the calculated $G^{(1)}$ will be both real-valued and symmetric, as the autocorrelation matrix is Hermitian. The eigenvalues and eigenvectors of a real symmetric matrix are also real, which explains why the mode amplitude functions shown in figures 3–6 are real-valued. As can be seen in figure 3, the utilization of a single-photon Fock state as the input reveals a linear system behavior, generating single-mode outputs for both r_{out} and l_{out} outputs. Any small-amplitude higher-order modes observed in this case can be attributed to minor numerical errors. In contrast, in all other cases where the input comprises multi-photon states, the system exhibits nonlinear behavior, leading to multi-mode outputs. This nonlinearity stems from the saturation of the emitter when exposed to light pulses containing more than one photon.

Due to the deterministic nature of the photon subtractor, if the duration of the input pulse is long enough based on the coupling strength of the emitter to the guided modes, a single photon is subtracted from all non-vacuum states at the input. Because of this, in figure 3, we assume a short pulse with $\tau = 1/\gamma_g$ so that there is still approximately half a photon at the right output, enabling us to explore the modal composition at this output as well. Otherwise, the single photon would be completely reflected, and there would be no photon in the right output mode. However, in all other figures throughout the paper, the pulse duration is assumed to be much longer than the radiation time of the atom to the waveguide, i.e. $\tau = 100/\gamma_g$. In figures 3–6, Part c illustrates the temporal intensity of the input and output pulses, representing their mean photon number distribution. In figure 3(c), due to the fast input pulse, it takes some

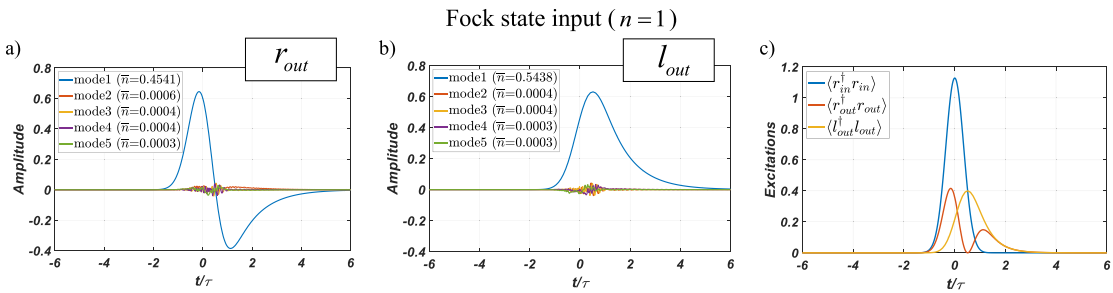

Figure 3. System output with a single-photon Fock state as input ($\tau = 1/\gamma_g$), showing (a) modal decomposition of the right (r_{out}) output mode, (b) modal decomposition of the left (l_{out}) output mode, and (c) temporal distribution of photons in input and output pulses.

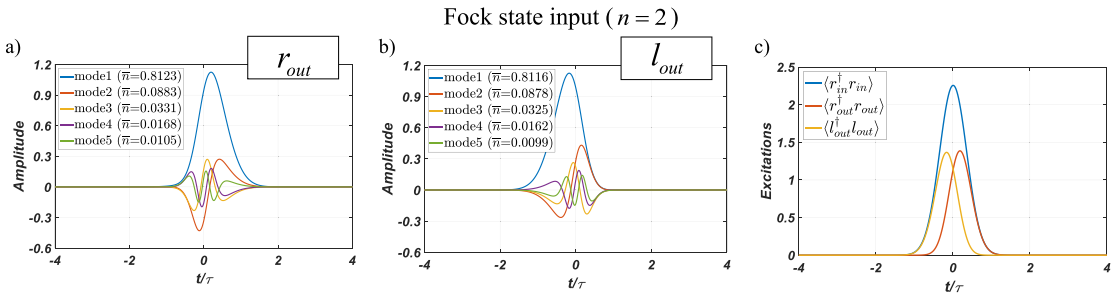

Figure 4. System output with a two-photon Fock state as input ($\tau = 100/\gamma_g$), showing (a) modal decomposition of the right (r_{out}) output mode, (b) modal decomposition of the left (l_{out}) output mode, and (c) temporal distribution of photons in input and output pulses.

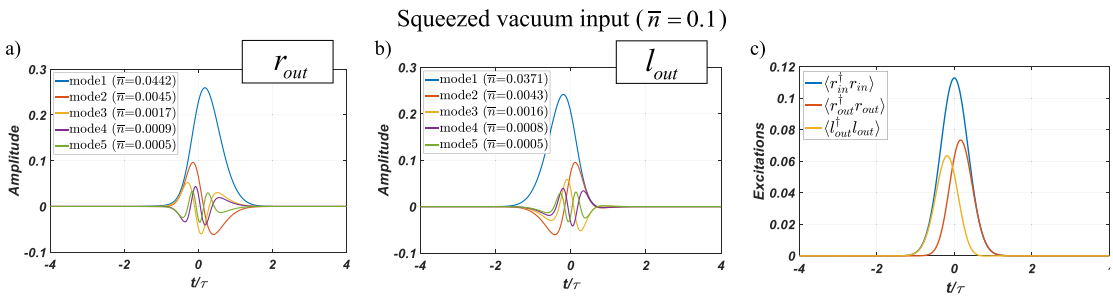

Figure 5. System output with a squeezed vacuum state with $\bar{n} = 0.1$ photons as input ($\tau = 100/\gamma_g$), showing (a) modal decomposition of the right (r_{out}) output mode, (b) modal decomposition of the left (l_{out}) output mode, and (c) temporal distribution of photons in input and output pulses.

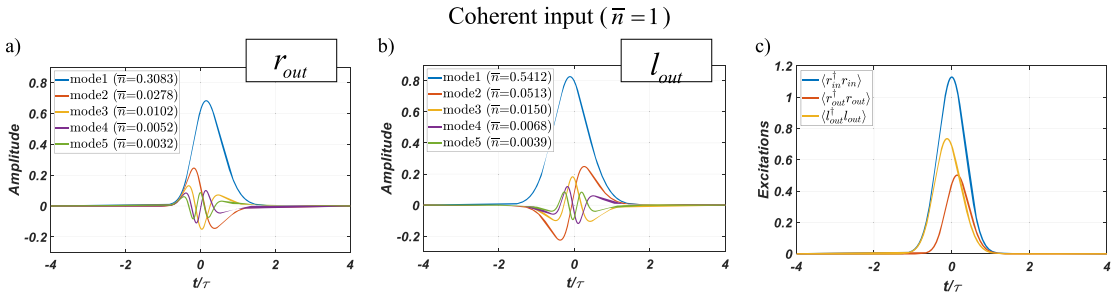

Figure 6. System output with a coherent state with $\bar{n} = 1$ photon as input ($\tau = 100/\gamma_g$), showing (a) modal decomposition of the right (r_{out}) output mode, (b) modal decomposition of the left (l_{out}) output mode, and (c) temporal distribution of photons in input and output pulses.

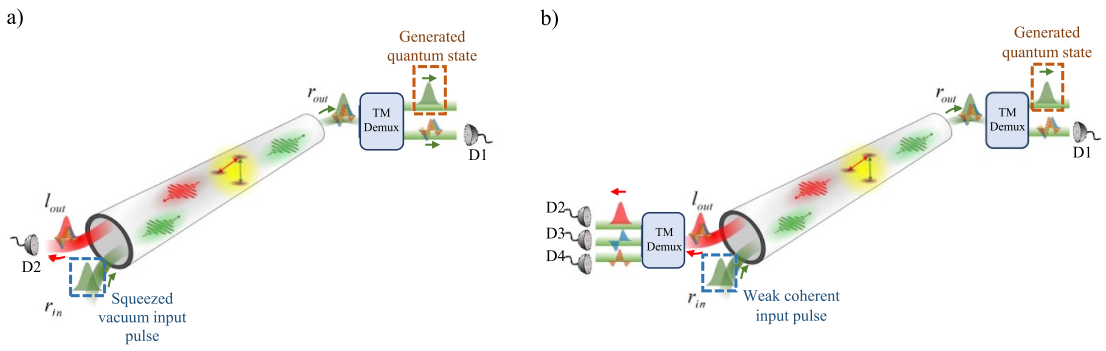

Figure 7. Proposed configurations for generation of single-mode non-Gaussian states from pulsed Gaussian input light (a) configuration with one demultiplexer and two detectors used for squeezed vacuum input pulses (b) configuration with two demultiplexers and four detectors used for coherent input pulses.

time for the emitter to initiate interaction with the light. Consequently, the r_{out} pulse leads compared to the l_{out} pulse. However, after the emitter becomes excited, it starts reflecting photons to the l_{out} mode, leading to a decrease in the intensity of the transmitted pulse. Additionally, both output pulses persist even after the input pulse vanishes, which is attributed to the time needed for the excited emitter to radiate photons to the guided modes. Conversely, as observed in the temporal intensity plots (part c) of the other three figures, the l_{out} pulse leads the r_{out} pulse. This implies that when the input pulse duration is sufficiently long, the subtractor subtracts the first arriving photon and subsequently allows other photons to transmit.

The subsequent step following this modal decomposition is to determine the quantum state of light that occupies the wavepackets corresponding to the calculated mode shapes. Given that our primary objective is to investigate the photon subtractor's potential for generating non-Gaussian states, we specifically concentrate on cases where the input to the system is of Gaussian type, namely the squeezed vacuum and coherent state inputs. While the presented photon subtractor operates deterministically, it can only subtract a photon if there is one present in the input, meaning that the input is not in the vacuum state. Therefore, for lightly squeezed vacuum states—such as those reported in [30]—as well as weak coherent pulses, containing a low mean photon number, there is still a high probability that no photon is subtracted. As a result, the process still needs to be heralded, where the detection of a photon at the l_{out} mode signals the successful subtraction of a photon and the potential generation of a non-Gaussian state.

Given that numerous applications in CV quantum optics rely on the utilization of single-mode non-Gaussian quantum states, we initially explore a configuration featuring a demultiplexing device at the r_{out} output. This device is a demultiplexer designed to effectively isolate the principal temporal mode from others, as depicted in figure 7(a). One experimental implementation for achieving this separation involves the utilization of quantum pulse gates (QPGs) [24]. A QPG operates through quantum frequency conversion in a nonlinear optical medium, where the input light interacts with a group-velocity-matched, shaped strong laser pulse. Depending on the medium's nonlinearity, this process can occur via either three-wave or four-wave mixing, translating the desired mode in the frequency domain to allow easy separation from the remaining light [31]. Initial experimental results for single-stage QPGs have demonstrated mode selectivity around 80% [32]. However, both theoretical and experimental studies have shown that cascading QPGs in a two-stage interferometric scheme can achieve near-unity conversion efficiency and selectivity [33, 34].

In the presented configuration, two detectors are utilized: detector D2 registers a click when a photon is successfully subtracted and directed to the l_{out} output, while detector D1 identifies the presence of photons in modes other than the principal mode of the r_{out} output. Now consider that a squeezed vacuum Gaussian pulse $|\zeta\rangle = \hat{S}(\zeta)|0\rangle$ is sent to r_{in} input and we want to study the generated quantum state in the principal mode of the r_{out} output. To model this problem, we need to consider a quantum network similar to the one shown in figure 2 with one virtual cavity at the input, one at the r_{out} output, and no cavity at the l_{out} output. The Hamiltonian of the system and Lindblad collapse operators corresponding to photon detection at detectors D1 and D2 will be as follows:

$$\begin{aligned} H(t) &= \frac{i}{2}\left[\sqrt{\gamma_g} g_\alpha(t)\, a_\alpha^\dagger \sigma_{13} + \sqrt{\gamma_g} g_\nu^*(t)\, \sigma_{31} a_\nu + g_\alpha(t)\, g_\nu^*(t)\, a_\alpha^\dagger a_\nu - \text{H.c.}\right] \\ L_0(t) &= \sqrt{\gamma_g}\sigma_{13} + g_\alpha^*(t)\, a_\alpha + g_\nu^*(t)\, a_\nu \qquad L_1(t) = \sqrt{\gamma_g}\sigma_{23} \end{aligned} \tag{18}$$

We employ the Monte Carlo wave-function method implemented in the QuTiP package in Python to simulate the described experimental scenario. Our focus is on the heralded (i.e. conditional on a detection

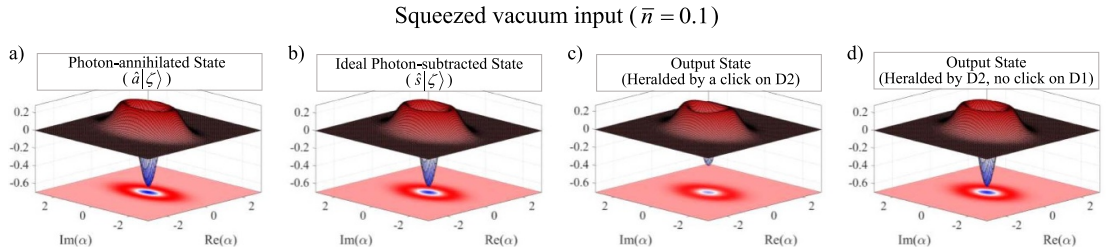

Figure 8. Photon subtraction results for a squeezed vacuum input $|\zeta\rangle$ with a mean photon number of $\bar{n} = 0.1$. The plots show the Wigner functions for (a) $\hat{a}\,|\zeta\rangle$, (b) $\hat{s}\,|\zeta\rangle$, (c) generated state by the proposed subtractor with no measurement performed by $D1$, (d) generated state by the proposed subtractor where both $D1$ and $D2$ are used for measurements according to the described scenario.

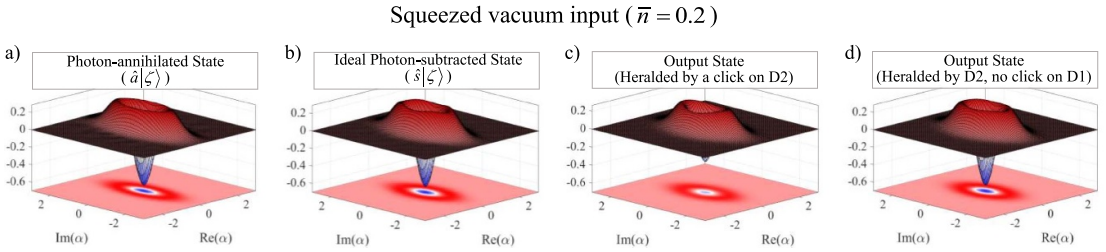

Figure 9. Photon subtraction results for a squeezed vacuum input $|\zeta\rangle$ with a mean photon number of $\bar{n} = 0.2$. The plots show the Wigner functions for (a) $\hat{a}\,|\zeta\rangle$, (b) $\hat{s}\,|\zeta\rangle$, (c) generated state by the proposed subtractor with no measurement performed by $D1$, (d) generated state by the proposed subtractor where both $D1$ and $D2$ are used for measurements according to the described scenario.

event) generation of the output quantum state in two specific cases. First, we explore the scenario where no measurement is performed using detector $D1$, while $D2$ heralds the successful subtraction of a photon. In the second case, we investigate the generated state signaled by a click on $D2$, with no concurrent click recorded by $D1$. The results are presented in figures 8 and 9 for two different input states with different squeezing levels containing mean number of photons $\bar{n} = 0.1$ and 0.2 (corresponding to $|\zeta| = 0.31$ and$|\zeta| = 0.43$), respectively. As seen in these figures, both measurement scenarios have resulted in the generation of non-Gaussian Wigner functions, reaching negative values and closely resembling the Wigner function of an odd Schrödinger's kitten state. The concept of generating Schrödinger's cat states by subtracting or adding single photons through traditional non-deterministic methods, equivalent to the implementation of photon annihilation and creation operators, has been explored for a long time [35]. For the sake of comparison, part a of the figures depicts the Wigner function of the state generated by applying the annihilation operator $\hat{a} = \sum_{n>0} \sqrt{n}\,|n-1\rangle\,\langle n|$. Additionally, by defining the ideal deterministic single photon subtractor as $\hat{s} = \sum_{n>0} |n-1\rangle\,\langle n|$, part b shows the result of applying this operator to the input state.

In figure 10, the fidelity of these generated states with the odd Schrödinger cat state $|\text{cat}_o\rangle = |\alpha\rangle - |-\alpha\rangle$ is plotted as a function of the amplitude α. As shown in this figure, while the first scenario, where no measurement is performed by detector $D1$, cannot surpass a fidelity of 90%, the second scenario generates cat states with an amplitude close to unity (given the level of squeezing) and achieves a fidelity approaching unity. While the non-deterministic method of photon subtraction can also theoretically generate cat states with fidelity approaching unity, it is important to note that this approach suffers from a significantly low success probability. This limitation arises from the use of beam splitters with very low reflectivity to suppress the subtraction of more than one photon. In contrast, the deterministic photon subtractor presented here can generate these states with much higher probabilities. Moreover, success probability increases as the level of squeezing in the input state rises. The success probabilities for the two cases studied here, with $|\zeta| = 0.31$ values of 0.1, are 4.3% and 3.5% for the scenarios described earlier. Similarly, for $|\zeta| = 0.43$, these success probabilities are 8.63% and 6.67%, respectively.

While squeezed states are indeed Gaussian states with positive Wigner functions throughout their phase space and exhibit classical-like properties such as well-defined phase and amplitude, they are not readily available experimentally. Their generation typically necessitates nonlinear interactions such as parametric down-conversion [36]. Conversely, the generation of few-photon coherent pulses is relatively straightforward, achieved through the appropriate attenuation of modulated laser beams. This highlights the significance of developing systems capable of directly generating exotic non-Gaussian states from coherent light. The coherent state is an eigenstate of the annihilation operator, implying that traditional

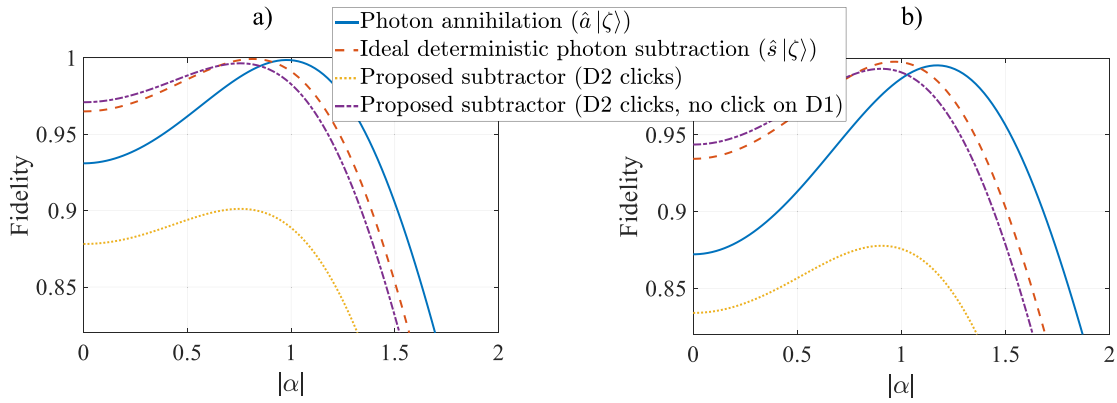

Figure 10. Fidelity between the generated states (obtained by applying different photon subtraction methods, as indicated in the plot legend) and odd Schrödinger's cat states of amplitude α. The input $|\zeta\rangle$is a squeezed vacuum state with mean photon numbers: (a) $\bar{n} = 0.1$ and (b) $\bar{n} = 0.2$.

beamsplitter-based photon subtraction does not alter the coherent input. Furthermore, an ideal deterministic photon subtractor (represented by the operator $\hat{s}$ defined above) when applied to a coherent state, while altering its photon number distribution, is still incapable of generating non-classical effects such as negative Wigner functions.

We thus aim to leverage the nonlinear multi-temporal mode nature of the SPRINT mechanism to explore the possibility of heralded generation of non-Gaussian states from a coherent input pulse. To achieve this, we consider the schematic setup configuration depicted in figure 7(b). In this setup, there are two demultiplexers at the two outputs of the photon subtractor, which separate the generated temporal modes. The first demultiplexer at the r_{out} output, similar to figure 7(a), only separates the principal mode, which contains the major part of the photons, from the other modes. The second demultiplexer at the lout output independently extracts the first three modes of the pulse. Three detectors ($D2$ to $D4$) are utilized at different outputs of this demultiplexer which allow us to determine the mode at which the subtracted photon exists. It is important to note that since the l_{out} output pulse cannot contain more than one photon in the deterministic photon subtraction, only one of the detectors can register a click. In our scenario, we explore the conditional generation of quantum states at the principal mode of the r_{out} output based on three different conditions. First, $D1$ registers no click, and $D2$ registers one. Second, $D1$ registers no click, and $D2$ registers one. Third, $D1$ registers no click, and $D3$ registers one.

To simulate the system, one can consider a quantum network again similar to the one shown in figure 2 but with three cascaded virtual cavities at the l_{out} output. Since here we are specifically interested in conditions where all the output photons go to the arranged cavities, and thus, no collapse occurs, it is possible to directly solve Schrödinger's equation $i\hbar\partial_t\,|\psi\rangle = H_{\text{eff}}|\psi\rangle$ using a time-dependent non-Hermitian effective Hamiltonian. The form of this Hamiltonian is given by $H_{\text{eff}} = H - i\hbar/2\left(L_0^\dagger L_0 + L_1^\dagger L_1\right)$, where the network Hamiltonian H and Lindblad operators L_0 and L_1 are derived in a manner similar to the explanation provided above equation (15) (See supplementary material of [25]). After determining the final density matrix $\rho = |\psi\rangle\langle\psi|$of the entire system, the quantum state stored in the r_{out} output cavity can be extracted by defining a suitable projection operator projecting the density matrix on a subspace based on the specified condition, which identifies the l_{out} cavity containing the subtracted photon. The density matrix of the resulting quantum state is obtained by projecting the overall density matrix using this operator, followed by a partial trace over the atomic state and the states of all cavities other than the one at r_{out} output. The outcomes of this simulation are depicted in parts a to c of figures 11 and 12 for coherent inputs with $\bar{n} = 1$ and 3 photons, respectively.

As depicted in these figures, when the subtracted photon is detected in the first mode of the l_{out} output, the resulting state closely resembles a coherent state. One the other hand, if the subtracted photon is found in the second mode, the output state resembles a displaced single-photon Fock state. However, when the photon is detected in the third mode, indicated by a click from detector $D4$, the generated state exhibits a Wigner function similar to that of a displaced cat state, represented by the form $\hat{D}(\gamma)\left[|\alpha\rangle + e^{i\beta}|-\alpha\rangle\right]$, where $\hat{D}$ is the displacement operator. Through optimization of the parameters α, β, and γ, we have identified the cat state that exhibits the highest fidelity with the state shown in part c of the figures. These optimized cat states are presented in part d of the figures, with their corresponding parameters detailed in the figure captions. Notably, the maximum fidelity achieved is 99.3% and 99.1% for the input coherent states with $\bar{n} = 1$ and 3

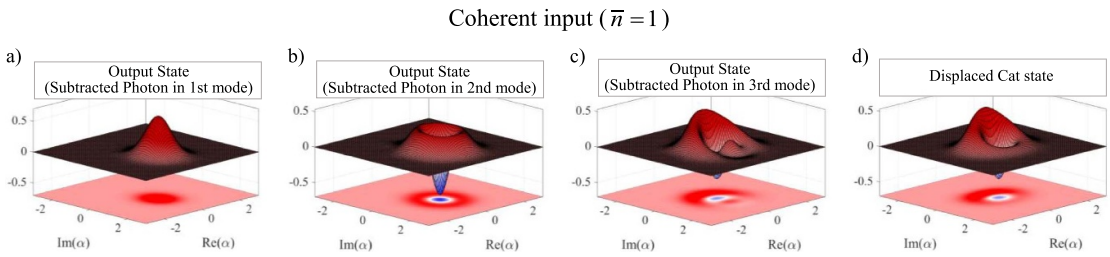

Figure 11. Photon subtraction results for a coherent input with a mean photon number of $\bar{n}=1$. The plots show the Wigner functions for (a) generated output state when the subtracted photon in detected in 1st mode, (b) generated output state when the subtracted photon in detected in 2nd mode, (c) generated output state when the subtracted photon in detected in 3rd mode, (d) a displaced cat state with parameters$\alpha=0.60$, $\beta=3.90$, $\gamma=0.07$.

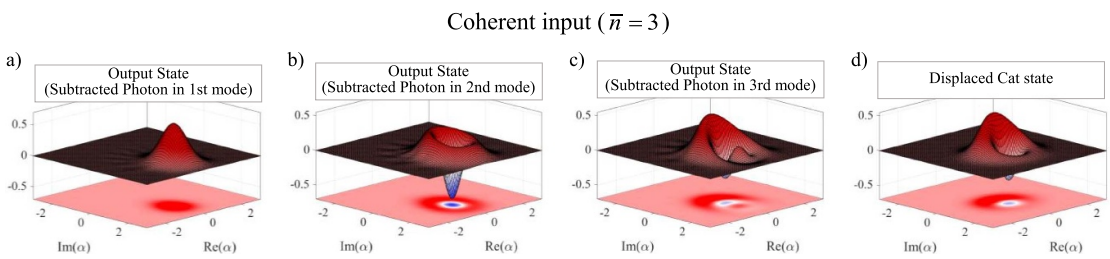

Figure 12. Photon subtraction results for a coherent input with a mean photon number of $\bar{n}=3$. The plots show the Wigner functions for (a) generated output state when the subtracted photon in detected in 1st mode, (b) generated output state when the subtracted photon in detected in 2nd mode, (c) generated output state when the subtracted photon in detected in 3rd mode, (d) a displaced cat state with parameters $\alpha=0.47$, $\beta=3.83$, $\gamma=0.56$.

photons, respectively. A further displacement of this generated states produces the Schrodinger's cat state which is a pivotal quantum source with numerous applications in quantum technology.

Successful interfacing of quantum emitters with chiral nanophotonic structures has been experimentally demonstrated across various platforms [37–43]. Achieving this requires high confinement levels to activate optical spin-orbit interactions, coupling light's polarization with its propagation direction [44]. Selective interaction of atomic transitions with photons of specific polarizations thereby creates a chiral light-matter system. The performance of these systems is commonly evaluated based on two factors. The first is the total coupling efficiency of each atomic transition to the waveguide, given by $\beta=\gamma/(\gamma+\Gamma)$, where γ is the total emission rate into both counterpropagating waveguide modes, and Γ accounts for all dissipative radiative and non-radiative channels. The second factor is the directionality of the coupling, defined as $F_{\mathrm{dir}}=\gamma_{\mathrm{dir}}/\gamma$, where γ_{dir} represents the emission rate into the desired propagation direction. Cold atoms coupled to the evanescent field of nanofibers have demonstrated directional emission into the guided modes [37]. In these systems, coupling efficiency can be enhanced by positioning the atoms closer to the fiber surface [45]. Higher coupling efficiencies can also be achieved by replacing the nanofiber with photonic crystal waveguides with reduced group velocity, which occurs when the guided mode frequency approaches the bandgap edge of the photonic structure [38]. Coupling efficiencies as high as $\beta=0.98$ have been reported when using quantum dots embedded within the waveguide and directly coupled to the waveguide field [39, 41]. Charged quantum dots possess a Λ-type energy level structure, making them promising candidates for single-photon Raman interactions. Their potential for deterministic single-photon subtraction has been previously studied [46]. Near-unity directionality has been achieved in both nanofiber and photonic crystal waveguide setups. Cesium cold atoms evanescently trapped on the surface of a nanofiber have demonstrated directional photon emission into the waveguide mode, with a directionality factor of $F_{\mathrm{dir}}=0.92$ [42]. Additionally, for quantum dots coupled to photonic crystal waveguides, directionality values as high as 0.98 have been reported [43]. According to these results, the high coupling and directionality reported specifically for solid-state systems make them potential candidates for implementing the photon subtraction scheme discussed in this paper.

4. Conclusion

In summary, we have demonstrated the potential of the deterministic single-photon subtraction scheme based on the single-photon Raman interaction effect in transforming squeezed and coherent states of light

into non-Gaussian states. We employed an input–output formalism with squeezed vacuum, coherent, and Fock state input pulses to calculate the temporal modes of the output light through eigen decomposition of first-order autocorrelation matrices. Subsequently, we determined the quantum state content of different modes by cascading virtual cavities at various outputs of the subtractor and evolving the obtained quantum network in time using quantum trajectory method. Our results revealed that the proposed scheme not only can achieve higher success probabilities for generating kitten states from squeezed vacuum compared to traditional beam-splitter-based methods but also has the capability to generate non-Gaussian states, including kitten states, directly from coherent laser pulses. The calculated fidelities are above 99% for both cases of squeezed and coherent states.

Data availability statement

All data that support the findings of this study are included within the article (and any supplementary files).

Funding

Canada First Research Excellence Fund-Transformative Quantum Technologies (CFREF-TQT).

Appendix A. Derivation of the optical Bloch equations

To find the set of governing Bloch equations given in equation (1), one must initially derive the total Hamiltonian of the system, which is the summation of the waveguide's Hamiltonian H_{wg}, emitter's Hamiltonian H_{e}, and their interaction Hamiltonian H_{int}:

$$H_{\mathrm{tot}} = H_{\mathrm{wg}} + H_{\mathrm{e}} + H_{\mathrm{int}} \tag{A.1}$$

where the different terms can be expressed as follows:

$$\begin{aligned} H_{\mathrm{wg}} &= \int_{-\infty}^{+\infty} \left(r_\omega^\dagger r_\omega - l_\omega^\dagger l_\omega\right) \omega \mathrm{d}\omega \\ H_{\mathrm{e}} &= \omega_1 \sigma_{33} + (\omega_1 - \omega_2)\, \sigma_{22} \\ H_{\mathrm{int}} &= iV_R \int_{-\infty}^{+\infty} \left(r_\omega^\dagger \sigma_{13} - \sigma_{31} r_\omega\right) \mathrm{d}\omega + iV_L \int_{-\infty}^{+\infty} \left(l_\omega^\dagger \sigma_{23} - \sigma_{32} l_\omega\right) \mathrm{d}\omega \end{aligned} \tag{A.2}$$

In the above equation, $\sigma_{ij} = |i\rangle\langle j|$ is the atomic transition operator, ω_i is the transition frequency from the excited state to the ground state $|i\rangle$, r_ω (l_ω) is the annihilation operator for a right (left) propagating mode of frequency ω, and V_R (V_L) is the coupling strength between the light propagating in right (left) direction with the corresponding atomic transition.

Heisenberg equation of motion can be used to obtain time derivatives of any arbitrary operator $A(t)$ in the Heisenberg picture ($\hbar = 1$):

$$\frac{\mathrm{d}A(t)}{\mathrm{d}t} = i\left[H_{\mathrm{tot}}, A(t)\right]. \tag{A.3}$$

This, after substituting in equations (A.1) and (A.2), results in the following set of ordinary differential equations governing time evolution of different atomic transition operators:

$$\dot{\sigma}_{11} = V_R \int_{-\infty}^{+\infty} \left(\sigma_{31} r_\omega + r_\omega^\dagger \sigma_{13}\right) \mathrm{d}\omega \qquad \dot{\sigma}_{13} = -i\omega_1 \sigma_{13} + V_R \int_{-\infty}^{+\infty} \left((\sigma_{33} - \sigma_{11})\, r_\omega\right) \mathrm{d}\omega - V_L \int_{-\infty}^{+\infty} \left(\sigma_{12} l_\omega\right) \mathrm{d}\omega$$

$$\dot{\sigma}_{22} = V_L \int_{-\infty}^{+\infty} \left(\sigma_{32} l_\omega + l_\omega^\dagger \sigma_{23}\right) \mathrm{d}\omega \qquad \dot{\sigma}_{23} = -i\omega_2 \sigma_{23} + V_L \int_{-\infty}^{+\infty} \left((\sigma_{33} - \sigma_{22})\, l_\omega\right) \mathrm{d}\omega - V_R \int_{-\infty}^{+\infty} \left(\sigma_{21} r_\omega\right) \mathrm{d}\omega$$

$$\dot{\sigma}_{33} = -V_R \int_{-\infty}^{+\infty} \left(r_\omega^\dagger \sigma_{13} + \sigma_{31} r_\omega\right) \mathrm{d}\omega \qquad \dot{\sigma}_{12} = -i\left(\omega_1 - \omega_2\right)\sigma_{12} + V_R \int_{-\infty}^{+\infty} \left(\sigma_{32} r_\omega\right) \mathrm{d}\omega + V_L \int_{-\infty}^{+\infty} \left(l_\omega^\dagger \sigma_{13}\right) \mathrm{d}\omega$$
$$- V_L \int_{-\infty}^{+\infty} \left(l_\omega^\dagger \sigma_{23} + \sigma_{32} l_\omega\right) \mathrm{d}\omega. \tag{A.4}$$

Also, for the right and left propagating field operators, one obtains:

$$\dot{r}_\omega = -i\omega r_\omega + V_R \sigma_{13} \qquad \dot{l}_\omega = i\omega l_\omega + V_L \sigma_{23} \tag{A.5}$$

which after integration gives:

$$r_\omega = r_\omega|_{t=t_0} \mathrm{e}^{-\mathrm{i}\omega\left(t-t_0\right)} + V_R \int_{t_0}^{t} \sigma_{13} \mathrm{e}^{-\mathrm{i}\omega\left(t-t'\right)} \mathrm{d}t' \qquad l_\omega = l_\omega|_{t=t_0} \mathrm{e}^{\mathrm{i}\omega\left(t-t_0\right)} + V_L \int_{t_0}^{t} \sigma_{23} \mathrm{e}^{-\mathrm{i}\omega\left(t-t'\right)} \mathrm{d}t'. \tag{A.6}$$

Substituting equations (A.6) into (A.4) results in the set of optical Bloch equations given in equation (1), where input operators r_{in} and l_{in} are defined as Fourier transform of the bath operators r_ω and l_ω at time $t = t_0$, before the light starts interacting with the emitter:

$$r_{\mathrm{in}}\left(t\right) := \frac{1}{\sqrt{2\pi}} \int_{-\infty}^{+\infty} \mathrm{d}\omega' r_{\omega'}\left(t_0\right) \mathrm{e}^{-\mathrm{i}\omega'\left(t-t_0\right)} \qquad l_{\mathrm{in}}\left(t\right) := \frac{1}{\sqrt{2\pi}} \int_{-\infty}^{+\infty} \mathrm{d}\omega' l_{\omega'}\left(t_0\right) \mathrm{e}^{\mathrm{i}\omega'\left(t-t_0\right)}. \tag{A.7}$$

In deriving equation (1), we assume that the coupling strengths V_R and V_L are equal and express them in terms of the emission rate γ_g of the atom to the guided modes of the waveguide as $V_R = V_L = \sqrt{\gamma_g/2\pi}$. Using a similar approach to equation (A.7), one can define the output operators r_{out} and l_{out} to keep track of the output light from the system at time $t = t_1$, which is after the interaction ends:

$$r_{\mathrm{out}}\left(t\right) = \frac{1}{\sqrt{2\pi}} \int_{-\infty}^{+\infty} \mathrm{d}\omega' r_{\omega'}\left(t_1\right) \mathrm{e}^{-\mathrm{i}\omega'\left(t-t_1\right)} \qquad l_{\mathrm{out}}\left(t\right) = \frac{1}{\sqrt{2\pi}} \int_{-\infty}^{+\infty} \mathrm{d}\omega' l_{\omega'}\left(t_1\right) \mathrm{e}^{\mathrm{i}\omega'\left(t-t_1\right)}. \tag{A.8}$$

Integrating equation (A.6) over all frequencies, and then substituting equations (A.7) and (A.8), yields the input–output relations for the system as given in equation (2).

Appendix B. Derivation of first autocorrelation matrices for squeezed vacuum input

When the input is in the squeezed vacuum state $|\zeta\rangle_0 = \hat{S}\left(\zeta\right)|0\rangle$ with the complex squeeze parameter $\zeta = se^{i\theta}$, we can define the state obtained by annihilating n photons from the original vacuum state as $|\zeta\rangle_n = a^n|\zeta\rangle_0$ where a is the annihilation operator of the corresponding mode. Then, using the notation ${}_i\langle\sigma_{ab}\rangle_j = {}_i\langle\zeta|\,\sigma_{ab}|\zeta\rangle_j$, we express the equations set (11) and (12) as follows:

$$\begin{aligned}
\partial_t\langle\sigma_{11}\rangle &= \sqrt{\gamma_g}\left({}_n\langle\sigma_{31}\rangle_{n+1}\,\alpha\left(t\right) + \alpha^*\left(t\right){}_{n+1}\langle\sigma_{13}\rangle_n\right) + \gamma_g\langle\sigma_{33}\rangle\\
\partial_t\langle\sigma_{33}\rangle &= -\sqrt{\gamma_g}\left({}_n\langle\sigma_{31}\rangle_{n+1}\,\alpha\left(t\right) + \alpha^*(t){}_{n+1}\langle\sigma_{13}\rangle_n\right) - 2\gamma_g\langle\sigma_{33}\rangle\\
\partial_t\langle\sigma_{13}\rangle &= \sqrt{\gamma_g}\left({}_n\langle\sigma_{33}\rangle_{n+1} - {}_n\langle\sigma_{11}\rangle_{n+1}\right)\alpha\left(t\right) - \gamma_g\langle\sigma_{13}\rangle\\
\partial_t\langle\sigma_{31}\rangle &= \sqrt{\gamma_g}\left({}_{n+1}\langle\sigma_{33}\rangle_n - {}_{n+1}\langle\sigma_{11}\rangle_n\right)\alpha^*\left(t\right) - \gamma_g\langle\sigma_{31}\rangle\\
\partial_t\langle\sigma_{32}\rangle &= -\sqrt{\gamma_g}{}_{n+1}\langle\sigma_{12}\rangle_n\alpha^*\left(t\right) - \gamma_g\langle\sigma_{32}\rangle\\
\partial_t\langle\sigma_{12}\rangle &= \sqrt{\gamma_g}{}_n\langle\sigma_{32}\rangle_{n+1}\alpha\left(t\right)
\end{aligned} \tag{B.1}$$

and:

$$\begin{aligned}
\partial_{t_2}\langle\sigma_{11}\left(t_2\right)\sigma_{13}\left(t_1\right)\rangle &= \sqrt{\gamma_g}\left({}_n\langle\sigma_{31}\left(t_2\right)\sigma_{13}\left(t_1\right)\rangle_{n+1}\,\alpha\left(t_2\right) + \alpha^*\left(t_2\right){}_{n+1}\langle\sigma_{13}\left(t_2\right)\sigma_{13}\left(t_1\right)\rangle_n\right) + \gamma_g\langle\sigma_{33}\left(t_2\right)\sigma_{13}\left(t_1\right)\rangle\\
\partial_{t_2}\langle\sigma_{33}\left(t_2\right)\sigma_{13}\left(t_1\right)\rangle &= -\sqrt{\gamma_g}\left({}_n\langle\sigma_{31}\left(t_2\right)\sigma_{13}\left(t_1\right)\rangle_{n+1}\,\alpha\left(t_2\right) + \alpha^*(t_2){}_{n+1}\langle\sigma_{13}\left(t_2\right)\sigma_{13}\left(t_1\right)\rangle_n\right)\\
&\quad - 2\gamma_g\langle\sigma_{33}\left(t_2\right)\sigma_{13}\left(t_1\right)\rangle\\
\partial_{t_2}\langle\sigma_{13}\left(t_2\right)\sigma_{13}\left(t_1\right)\rangle &= \sqrt{\gamma_g}\left({}_n\langle\sigma_{33}\left(t_2\right)\sigma_{13}\left(t_1\right)\rangle_{n+1} - {}_n\langle\sigma_{11}\left(t_2\right)\sigma_{13}\left(t_1\right)\rangle_{n+1}\right)\alpha\left(t_2\right) - \gamma_g\langle\sigma_{13}\left(t_2\right)\sigma_{13}\left(t_1\right)\rangle\\
\partial_{t_2}\langle\sigma_{31}\left(t_2\right)\sigma_{13}\left(t_1\right)\rangle &= \sqrt{\gamma_g}\left({}_{n+1}\langle\sigma_{33}\left(t_2\right)\sigma_{13}\left(t_1\right)\rangle_n - {}_{n+1}\langle\sigma_{11}\left(t_2\right)\sigma_{13}\left(t_1\right)\rangle_n\right)\alpha^*\left(t_2\right) - \gamma_g\langle\sigma_{31}\left(t_2\right)\sigma_{13}\left(t_1\right)\rangle\\
\partial_{t_2}\langle\sigma_{32}\left(t_2\right)\sigma_{23}\left(t_1\right)\rangle &= -\sqrt{\gamma_g}{}_{n+1}\langle\sigma_{12}\left(t_2\right)\sigma_{23}\left(t_1\right)\rangle_n\alpha^*\left(t_2\right) - \gamma_g\langle\sigma_{32}\left(t_2\right)\sigma_{23}\left(t_1\right)\rangle\\
\partial_{t_2}\langle\sigma_{12}\left(t_2\right)\sigma_{23}\left(t_1\right)\rangle &= \sqrt{\gamma_g}{}_n\langle\sigma_{32}\left(t_2\right)\sigma_{23}\left(t_1\right)\rangle_{n+1}\alpha\left(t_2\right)
\end{aligned} \tag{B.2}$$

Both equations (B.1) and (B.2) represent sets of recurrence equations, similar to the case of Fock state input. As n increases, $|\zeta\rangle_n$ tends toward zero, allowing for truncation at a sufficiently large n, after which the equations can be solved. The initial conditions for equation (B.2) are analogous to those provided in equation (13). Furthermore, in accordance with the photon number distribution of the squeezed vacuum state, which is as follows:

$$|\zeta\rangle = \sum_n \frac{\left(-e^{i\theta}\tanh s\right)^n}{\sqrt{\cosh s}} \frac{(2n!)^{\frac{1}{2}}}{2^n n!} |2n\rangle. \tag{B.3}$$

The nonzero initial conditions for equation (B.1) will be:

$$\begin{aligned} {}_i\langle\sigma_{11}\rangle_j &= \sum_n \frac{\left(-e^{i\theta}\tanh s\right)^{2n+\frac{i+j}{2}+1}}{\cosh s} \left[\frac{\left(2\left(n+\frac{i+1}{2}\right)!\right)\left(2\left(n+\frac{j+1}{2}\right)!\right)}{2^{2n+\frac{i+j}{2}+1}\left(n+\frac{i+1}{2}\right)!\left(n+\frac{j+1}{2}\right)!(2n+1)!}\right] \quad i \text{ and } j \text{ are both odd} \\ {}_i\langle\sigma_{11}\rangle_j &= \sum_n \frac{\left(-e^{i\theta}\tanh s\right)^{2n+\frac{i+j}{2}}}{\cosh s} \left[\frac{((2n+i)!)((2n+j)!)}{2^{2n+\frac{i+j}{2}}\left(n+\frac{i}{2}\right)!\left(n+\frac{j}{2}\right)!(2n)!}\right] \quad i \text{ and } j \text{ are both even} \end{aligned}. \tag{B.4}$$

Solving equation (B.2) gives the first correlation terms appearing on the right-hand side of equation (8). For the other three correlation terms appeared in equation (8), one can write:

$$\begin{aligned} \left\langle r_{\text{in}}{}^{\dagger}(t_2)\, r_{\text{in}}(t_1)\right\rangle &= \left(\sum_n \frac{\left(-e^{i\theta}\tanh s\right)^{2n+2}}{\cosh s}\left[\frac{(2(n+1)!)^2}{2^{2n+2}((n+1)!)^2(2n+1)!}\right]\right)\alpha^*(t_2)\,\alpha(t_1) \\ \left\langle r_{\text{in}}{}^{\dagger}(t_2)\,\sigma_{13}(t_1)\right\rangle &= \alpha^*(t_2)\,{}_1\langle\sigma_{13}(t_1)\rangle_0 \\ \langle\sigma_{31}(t_2)\, r_{\text{in}}(t_1)\rangle &= {}_0\langle\sigma_{31}(t_2)\rangle_1\,\alpha(t_1) \end{aligned}. \tag{B.5}$$

Appendix C. Derivation of first autocorrelation matrices for coherent input

For the case where the input pulse is in a coherent state $|\alpha\rangle$, one has $r_{\text{in}}(t)|\alpha\rangle = \alpha(t)|\alpha\rangle$. Taking the expectation values of both sides of equation (1) yields:

$$\begin{aligned} \partial_t\langle\sigma_{11}\rangle &= \sqrt{\gamma_g}\left(\langle\sigma_{31}\rangle\alpha(t) + \alpha^*(t)\langle\sigma_{13}\rangle\right) + \gamma_g\langle\sigma_{33}\rangle \\ \partial_t\langle\sigma_{33}\rangle &= -\sqrt{\gamma_g}\left(\langle\sigma_{31}\rangle\alpha(t) + \alpha^*(t)\langle\sigma_{13}\rangle\right) - 2\gamma_g\langle\sigma_{33}\rangle \\ \partial_t\langle\sigma_{13}\rangle &= \sqrt{\gamma_g}\left(\langle\sigma_{33}\rangle - \langle\sigma_{11}\rangle\right)\alpha(t) - \gamma_g\langle\sigma_{13}\rangle \\ \partial_t\langle\sigma_{31}\rangle &= \sqrt{\gamma_g}\alpha^*(t)\left(\langle\sigma_{33}\rangle - \langle\sigma_{11}\rangle\right) - \gamma_g\langle\sigma_{31}\rangle \\ \partial_t\langle\sigma_{32}\rangle &= -\sqrt{\gamma_g}\alpha^*(t)\langle\sigma_{12}\rangle - \gamma_g\langle\sigma_{32}\rangle \\ \partial_t\langle\sigma_{12}\rangle &= \sqrt{\gamma_g}\langle\sigma_{32}\rangle\alpha(t) \end{aligned} \tag{C.1}$$

which needs to be solved according to the initial condition of $\langle\sigma_{11}\rangle = 1$. Equation (12) in this case changes to the following form:

$$\begin{aligned} \partial_{t_2}\langle\sigma_{11}(t_2)\sigma_{13}(t_1)\rangle &= \sqrt{\gamma_g}\left(\langle\sigma_{31}(t_2)\sigma_{13}(t_1)\rangle\alpha(t_2) + \alpha^*(t_2)\langle\sigma_{13}(t_2)\sigma_{13}(t_1)\rangle\right) + \gamma_g\langle\sigma_{33}(t_2)\sigma_{13}(t_1)\rangle \\ \partial_{t_2}\langle\sigma_{33}(t_2)\sigma_{13}(t_1)\rangle &= -\sqrt{\gamma_g}\left(\langle\sigma_{31}(t_2)\sigma_{13}(t_1)\rangle\alpha(t_2) + \alpha^*(t_2)\langle\sigma_{13}(t_2)\sigma_{13}(t_1)\rangle\right) - 2\gamma_g\langle\sigma_{33}(t_2)\sigma_{13}(t_1)\rangle \\ \partial_{t_2}\langle\sigma_{13}(t_2)\sigma_{13}(t_1)\rangle &= \sqrt{\gamma_g}\left(\langle\sigma_{33}(t_2)\sigma_{13}(t_1)\rangle\alpha(t_2) - \alpha^*(t_2)\langle\sigma_{11}(t_2)\sigma_{13}(t_1)\rangle\right) - \gamma_g\langle\sigma_{13}(t_2)\sigma_{13}(t_1)\rangle \\ \partial_{t_2}\langle\sigma_{31}(t_2)\sigma_{13}(t_1)\rangle &= \sqrt{\gamma_g}\left(\langle\sigma_{33}(t_2)\sigma_{13}(t_1)\rangle - \langle\sigma_{11}(t_2)\sigma_{13}(t_1)\rangle\right)\alpha^*(t_2) - \gamma_g\langle\sigma_{31}(t_2)\sigma_{13}(t_1)\rangle \\ \partial_{t_2}\langle\sigma_{32}(t_2)\sigma_{23}(t_1)\rangle &= -\sqrt{\gamma_g}\langle\sigma_{12}(t_2)\sigma_{23}(t_1)\rangle\alpha^*(t_2) - \gamma_g\langle\sigma_{32}(t_2)\sigma_{23}(t_1)\rangle \\ \partial_{t_2}\langle\sigma_{12}(t_2)\sigma_{23}(t_1)\rangle &= \sqrt{\gamma_g}\langle\sigma_{32}(t_2)\sigma_{23}(t_1)\rangle\alpha(t_2) \end{aligned}. \tag{C.2}$$

The initial conditions will be as follows:

$$\begin{aligned} \langle\sigma_{32}(t_2)\sigma_{23}(t_1)\rangle|_{t_2=t_1} &= \langle\sigma_{31}(t_2)\sigma_{13}(t_1)\rangle|_{t_2=t_1} = \langle\sigma_{33}(t_1)\rangle \\ \langle\sigma_{12}(t_2)\sigma_{23}(t_1)\rangle|_{t_2=t_1} &= \langle\sigma_{11}(t_2)\sigma_{13}(t_1)\rangle|_{t_2=t_1} = \langle\sigma_{13}(t_1)\rangle \end{aligned}. \tag{C.3}$$

Solving equation (C.2) with the initial conditions given in equation (C.3) gives the first correlation terms appearing on the right-hand side of equation (8). Also, the other correlation terms appearing in equation (8) will be:

$$\begin{aligned}
&\left\langle {r_{\text{in}}}^{\dagger}\left(t_2\right) r_{\text{in}}\left(t_1\right)\right\rangle = \alpha^{*}\left(t_2\right)\alpha\left(t_1\right)\\
&\left\langle {r_{\text{in}}}^{\dagger}\left(t_2\right)\sigma_{13}\left(t_1\right)\right\rangle = \alpha^{*}\left(t_2\right)\left\langle\sigma_{13}\left(t_1\right)\right\rangle.\\
&\left\langle\sigma_{31}\left(t_2\right) r_{\text{in}}\left(t_1\right)\right\rangle = \left\langle\sigma_{31}\left(t_2\right)\right\rangle\alpha\left(t_1\right)
\end{aligned} \tag{C.4}$$

References

[1] Braunstein S L and Van Loock P 2005 Quantum information with continuous variables *Rev. Mod. Phys.* **77** 513
[2] Xu F, Curty M, Qi B, Qian L and Lo H-K 2015 Discrete and continuous variables for measurement-device-independent quantum cryptography *Nat. Photon.* **9** 772–3
[3] Choe S 2022 Quantum computing overview: discrete vs. continuous variable models (arXiv:2206.07246)
[4] Zhang Z and Zhuang Q 2021 Distributed quantum sensing *Quantum Sci. Technol.* **6** 043001
[5] Lvovsky A, Grangier P, Ourjoumtsev A, Parigi V, Sasaki M and Tualle-Brouri R 2020 Production and applications of non-Gaussian quantum states of light (arXiv:2006.16985)
[6] Niset J, Fiurášek J and Cerf N J 2009 No-go theorem for Gaussian quantum error correction *Phys. Rev. Lett.* **102** 120501
[7] Lund A P, Ralph T C and Haselgrove H L 2008 Fault-tolerant linear optical quantum computing with small-amplitude coherent states *Phys. Rev. Lett.* **100** 030503
[8] Takahashi H, Neergaard-Nielsen J S, Takeuchi M, Takeoka M, Hayasaka K, Furusawa A and Sasaki M 2010 Entanglement distillation from Gaussian input states *Nat. Photon.* **4** 178–81
[9] Eisert J, Scheel S and Plenio M B 2002 Distilling Gaussian states with Gaussian operations is impossible *Phys. Rev. Lett.* **89** 137903
[10] Goncharov R, Kiselev A D, Moiseev E, Samsonov E, Moiseev S, Kiselev F and Egorov V 2023 Quantum repeaters and teleportation via entangled phase-modulated multimode coherent states *Phys. Rev. Appl.* **20** 044030
[11] Jeong H, Zavatta A, Kang M, Lee S-W, Costanzo L S, Grandi S, Ralph T C and Bellini M 2014 Generation of hybrid entanglement of light *Nat. Photon.* **8** 564–9
[12] Hertz A and Bièvre S D 2022 Decoherence and nonclassicality of photon-added/subtracted multi-mode Gaussian states (arXiv:2204.06358)
[13] Kumar R, Barrios E, Kupchak C and Lvovsky A 2013 Experimental characterization of bosonic creation and annihilation operators *Phys. Rev. Lett.* **110** 130403
[14] Dakna M, Clausen J, Knöll L and Welsch D-G 1999 Generation of arbitrary quantum states of traveling fields *Phys. Rev.* A **59** 1658
[15] Fiurášek J, García-Patrón R and Cerf N J 2005 Conditional generation of arbitrary single-mode quantum states of light by repeated photon subtractions *Phys. Rev.* A **72** 033822
[16] Wenger J, Tualle-Brouri R and Grangier P 2004 Non-Gaussian statistics from individual pulses of squeezed light *Phys. Rev. Lett.* **92** 153601
[17] Ourjoumtsev A, Tualle-Brouri R, Laurat J and Grangier P 2006 Generating optical Schrodinger kittens for quantum information processing *Science* **312** 83–86
[18] Rosenblum S, Bechler O, Shomroni I, Lovsky Y, Guendelman G and Dayan B 2016 Extraction of a single photon from an optical pulse *Nat. Photon.* **10** 19–22
[19] Honer J, Löw R, Weimer H, Pfau T and Büchler H P 2011 Artificial atoms can do more than atoms: deterministic single photon subtraction from arbitrary light fields *Phys. Rev. Lett.* **107** 093601
[20] Sarkar S 2021 *Creating and Shaping Light at Single Photon Level* (University of Waterloo)
[21] Pasharavesh A and Bajcsy M 2024 Deterministic single photon subtraction with a cascade of waveguide-coupled atoms *Opt. Express* **32** 26740–50
[22] Rosenblum S, Borne A and Dayan B 2014 Analysis of photonic quantum nodes based on single photon Raman interaction (arXiv:1412.0604)
[23] Brecht B, Reddy D V, Silberhorn C and Raymer M G 2015 Photon temporal modes: a complete framework for quantum information science *Phys. Rev.* X **5** 041017
[24] Raymer M G and Walmsley I A 2020 Temporal modes in quantum optics: then and now *Phys. Scr.* **95** 064002
[25] Kiilerich A H and Mølmer K 2019 Input-output theory with quantum pulses *Phys. Rev. Lett.* **123** 123604
[26] Loudon R 2000 *The Quantum Theory of Light* (OUP Oxford)
[27] Breuer H-P and Petruccione F 2002 *The Theory of Open Quantum Systems* (Oxford University Press)
[28] Walls D and Milburn G J 2008 Input–output formulation of optical cavities *Quantum Optics* (Springer) pp 127–41
[29] Combes J, Kerckhoff J and Sarovar M 2017 The SLH framework for modeling quantum input-output networks *Adv. Phys.* X **2** 784–888
[30] Takanashi N, Inokuchi W, Serikawa T and Furusawa A 2019 Generation and measurement of a squeezed vacuum up to 100 MHz at 1550 nm with a semi-monolithic optical parametric oscillator designed towards direct coupling with waveguide modules *Opt. Express* **27** 18900–9
[31] Ansari V, Donohue J M, Allgaier M, Sansoni L, Brecht B, Roslund J, Treps N, Harder G and Silberhorn C 2018 Tomography and purification of the temporal-mode structure of quantum light *Phys. Rev. Lett.* **120** 213601
[32] Brecht B, Eckstein A, Ricken R, Quiring V, Suche H, Sansoni L and Silberhorn C 2014 Demonstration of coherent time-frequency Schmidt mode selection using dispersion-engineered frequency conversion *Phys. Rev.* A **90** 030302
[33] Reddy D V, Raymer M G and McKinstrie C J 2014 Efficient sorting of quantum-optical wave packets by temporal-mode interferometry *Opt. Lett.* **39** 2924–7
[34] Reddy D V and Raymer M G 2018 High-selectivity quantum pulse gating of photonic temporal modes using all-optical Ramsey interferometry *Optica* **5** 423–8
[35] Marco B and Alessandro Z 2010 *Progress in Optics* (Elsevier) pp 41–83
[36] Andersen U L, Gehring T, Marquardt C and Leuchs G 2016 30 years of squeezed light generation *Phys. Scr.* **91** 053001

[37] Petersen J, Volz J and Rauschenbeutel A 2014 Chiral nanophotonic waveguide interface based on spin-orbit interaction of light *Science* **346** 67–71
[38] Hood J D, Goban A, Asenjo-Garcia A, Lu M, Yu S-P, Chang D E and Kimble H 2016 Atom–atom interactions around the band edge of a photonic crystal waveguide *Proc. Natl Acad. Sci.* **113** 10507–12
[39] Arcari M *et al* 2014 Near-unity coupling efficiency of a quantum emitter to a photonic crystal waveguide *Phys. Rev. Lett.* **113** 093603
[40] Liedl C, Tebbenjohanns F, Bach C, Pucher S, Rauschenbeutel A and Schneeweiss P 2024 Observation of superradiant bursts in a cascaded quantum system *Phys. Rev.* X **14** 011020
[41] Reichert T, Lichtmannecker S, Reithmaier G, Zeitlmair M, Wembacher J, Rauscher A, Bichler M, Müller K, Kaniber M and Finley J J 2014 Highly directed emission from self-assembled quantum dots into guided modes in disordered photonic-crystal waveguides *Phys. Rev.* B **90** 115310
[42] Mitsch R, Sayrin C, Albrecht B, Schneeweiss P and Rauschenbeutel A 2014 Quantum state-controlled directional spontaneous emission of photons into a nanophotonic waveguide *Nat. Commun.* **5** 5713
[43] Söllner I *et al* 2015 Deterministic photon–emitter coupling in chiral photonic circuits *Nat. Nanotechnol.* **10** 775–8
[44] Lodahl P, Mahmoodian S, Stobbe S, Rauschenbeutel A, Schneeweiss P, Volz J, Pichler H and Zoller P 2017 Chiral quantum optics *Nature* **541** 473–80
[45] Chang D, Douglas J, González-Tudela A, Hung C-L and Kimble H 2018 Colloquium: quantum matter built from nanoscopic lattices of atoms and photons *Rev. Mod. Phys.* **90** 031002
[46] Du J, Li W and Bajcsy M 2020 Deterministic single-photon subtraction based on a coupled single quantum dot-cavity system *Opt. Express* **28** 6835–45